

Analysis of size effects on the geomechanical parameters of intact granite samples under unconfined conditions

J. Quiñones¹ · J. Arzúa² · L. R. Alejano¹ · F. García-Bastante¹ · D. Mas Ivars³ · G. Walton⁴

Received: 30 August 2016 / Accepted: 21 February 2017 / Published online: 7 March 2017
© Springer-Verlag Berlin Heidelberg 2017

Abstract A total of 28 uniaxial compressive strength tests were performed on cylindrical Blanco Mera granite samples with diameters ranging between 14 and 100 mm, with results indicating that this granite undergoes a significant reverse size effect: the UCS increases as sample diameter increases up to 54 mm, but thereafter decreases. It was also found that the results tend to be more scattered for smaller sample diameters. We also found an apparent correlation between Young's modulus and sample diameter. It was not possible to draw any clear conclusions regarding the variability in Poisson's ratio with sample size. With respect to crack initiation and crack damage stresses, the behaviour of the tested samples also indicates a reverse effect. This research would suggest that the traditionally assumed decrease in strength as sample size increases does not hold for granite samples with diameters below 54 mm.

Keywords Compressive strength · Granite · Intact rock · Size effect

1 Introduction and aims

Geological–genetic conditions, natural phenomena (weathering and tectonic action) and hydrologic, chemical and thermal processes are the causes of the essentially inhomogeneous and discontinuous nature of rocks and rock masses at both the macroscopic and microscopic scales. Consequently, it comes as no surprise that the results of in situ and laboratory mechanical tests on rock—besides being site-specific—are dependent on the dimensions of the tested volumes, in terms of both average values and variability. Although size effects on rock, joint and rock mass properties have been widely investigated in rock engineering practice, in the absence of a comprehensive understanding of these effects, engineering judgement is required to extrapolate test data to the in situ scale of rock engineering projects.

Early studies of size effects on rock strength were carried out by Bieniawski [8] (coal pillar samples) and by Pratt et al. [51] and Hoek and Brown [26] (hard rock samples). Further insights, based on information compiled at two International Workshops on Scale Effects in Rock Masses (held in Loen, Norway, and in Lisbon, Portugal in 1990 and 1993, respectively), served to establish a basic understanding of scale effects in rock mechanics. Subsequent investigations by a number of authors (Hawkins [25], Yoshinaka et al. [61], Pierce et al. [49]) established that size effects vary significantly by rock type, depending on strength, texture, micro-flaws (pores, open cracks and veins), weathering/alteration and spatial variations in micro-properties.

On the basis of a number of studies of uniaxial compression tests, Masoumi et al. [44] suggested that the size-effect behaviour of small samples does not follow the widely accepted size-effect model whereby strength

✉ L. R. Alejano
alejano@uvigo.es

¹ Natural Resources and Environmental Engineering Department, University of Vigo, Vigo, Spain

² Department of Metallurgical and Mining Engineering, Universidad Católica del Norte, Antofagasta, Chile

³ Swedish Nuclear Fuel and Waste Management Co, SKB, Stockholm, Sweden

⁴ Department of Geology and Geological Engineering, Colorado School of Mines, Golden, CO, USA

decreases monotonically as sample size increases—an important observation that had not been considered in earlier investigations (Hoek and Brown [26]). Masoumi et al. [44] conducted comprehensive analytical research to assess this behaviour, but only in samples of sandstone. The aim of this study is, therefore, to complement the findings of Masoumi et al. [44] by studying size effects in hard rock.

We report results of uniaxial compressive strength (UCS) tests on different-sized samples of Blanco Mera granite in order to evaluate size effects on geomechanical parameters of this rock. Our findings should contribute to the development of realistic scaling laws and serve as the basis for calibrating numerical models.

2 Size effects on strength

As background for this study, below we review knowledge to date on the behaviour of rocks during compression testing, including diverse perspectives on size effects.

2.1 Compressive failure in brittle rock

Probably the most widely used measure of rock strength is to determine uniaxial (or unconfined) compression strength and elastic parameters (Young's modulus and Poisson's ratio) from cylindrical samples prepared from drilled cores from intact rock. The response to testing depends on the nature and composition of the rock and on the condition of the test samples. All other factors remaining constant, the strength of a given sample will weaken as the number of flaws increases (e.g. weathering defects, pores and pre-existing micro-cracks).

Following International Society for Rock Mechanics (ISRM) [27] guidelines, to determine the compressive behaviour of rock samples, axial and lateral strains, ε_1 and ε_3 , respectively, are recorded using a constant zero or nonzero confining stress. The stress–strain path to failure can thus be fully visualized when axial, lateral and volumetric strains are plotted against axial stress (Fig. 1).

Martin [40] provided an explanation for the inelastic effects that can be observed in UCS testing, arguing that the stress–strain curves for a brittle material can be divided into five regions (Fig. 1). The terminology used below is that of Diederichs and Martin [14]. Note that rock post-peak strength, after σ_c or UCS, which marks the beginning of post-peak behaviour (region V), is beyond the scope of this study.

The initial region of the stress–strain curve represents closure in the sample of pre-existing micro-cracks oriented normal to the principal stress (region I). Once these cracks are closed (σ_{cc}), the rock tends to behave in a linear,

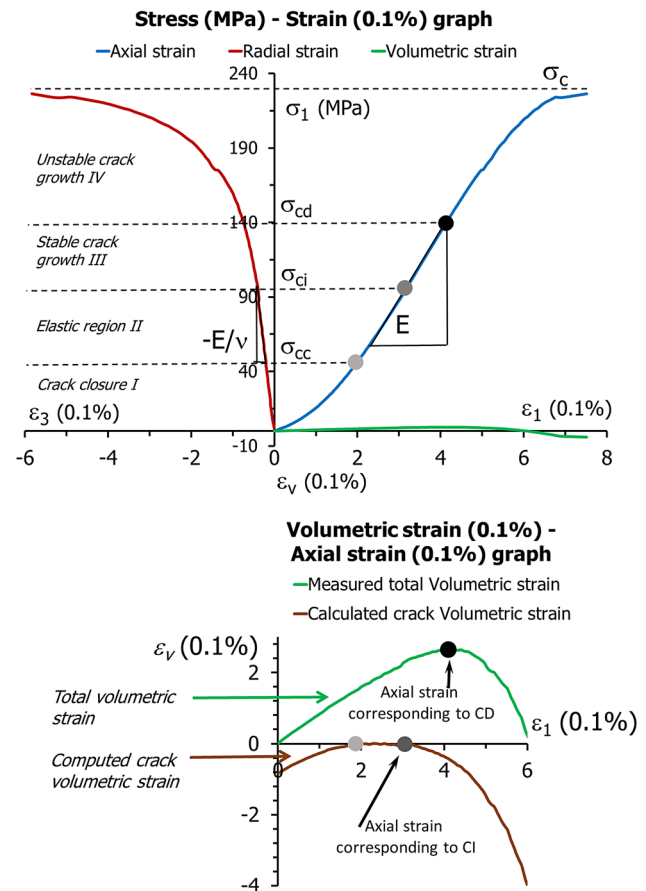


Fig. 1 Stress–strain diagram obtained from a single UCS test. Based on Martin [40]

homogenous and elastic manner until crack initiation (CI or σ_{ci}) stress is reached (region II) and, hence, elastic properties can be determined. This behaviour has been attributed to the deformation-stress memory of rock. The fatigue lifecycle of a rock is short because of high stress concentrations at the extreme ends of micro-cracks and flaws generated by thermal fluctuations or external loading during geological development [32]. According to Masoumi [43], stress concentration effects can also contribute to the concave shape of the initial part of the axial stress–axial strain curve.

Stable crack growth (region III) occurs when new axial micro-cracks begin to appear, in line with Griffith's theory [22] stating that the tensile fracture of a brittle material initiates with microscopic flaws. Griffith [22] suggested that these micro-cracks are the result of intense tensile stress concentrations near the extreme ends of microscopic elliptical flaws. Several researchers [9, 23] have demonstrated that, although cracks do start to form at axial stresses equal to about $8 \sigma_t$ (in line with Griffith's theory [22]), this form of cracking is stable. In other words, additional loading would be necessary to extend the cracks.

The main feature of stable crack growth is that the cracks tend to open parallel to the direction of the maximum compressive load; consequently, only the lateral gauge registers the associated inelastic deformation. Although it is difficult to directly estimate CI from the stress–strain curves, it is possible to identify where it occurs by plotting crack volumetric strain against axial strain. To calculate crack volumetric strain, elastic volumetric strain (Eq. 1) is first calculated using the elastic constants (E, ν) determined from the elastic portion of the stress–strain curve:

$$\varepsilon_{v\text{elastic}} = \frac{1 - 2\nu}{E} (\sigma_1 - \sigma_3) \quad (1)$$

The elastic volumetric strain is then subtracted from the total volumetric strain to determine the inelastic volumetric strain (i.e. the volumetric strain associated with the cracks):

$$\varepsilon_v = \varepsilon_1 + 2\varepsilon_3 \quad (2)$$

CI is thus the stress level at which inelastic expansion begins (i.e. systematic micro-fracturing), representing the first stage of stress-induced damage in low-porosity rocks—as shown in the plotted crack volumetric strain line in Fig. 1 [24, 40]. CI, identified as the point where the lateral and volumetric strain curves depart from linearity, represents the transition from linear elastic behaviour to stable crack growth in the stress–strain behaviour of intact rock. It has been pointed to as a key parameter in studies of brittle rock deformation and fracturing characteristics by several authors [9, 24, 37, 41, 60]. CI is also used in practice to estimate potential spalling in underground excavations in massive hard rock masses [14].

Although it is difficult to define a method to accurately compute where departure from linearity occurs, various approaches have been proposed in the literature to estimate the value of CI. These include volumetric strain methods [10, 40, 41], lateral strain methods [13, 37] and acoustic emission methods [17, 20, 63]. Notably, Nicksiar and Martin [46] assessed the strain methods for hard-brittle diorite samples, concluding that each provided consistent and accurate results. Since no suggested method has so far been proposed by the ISRM [27], the crack volumetric strain reversal approach as described by Martin and Chandler [41] is followed in this study.

Finally, the axial stress point at which nonlinearity begins in the axial stress–axial strain curve—called the crack damage (CD or σ_{cd}) point—marks the onset of unstable crack growth (region IV). Because onset of nonlinearity is often very subtle, it is useful to use the total volumetric strain reversal point as an indicator of CD (they coincide under unconfined conditions). CD usually occurs at stress levels of around 65–85% of peak strength (Fig. 1). Further loading above this stress level results in permanent

damage to the material, since, after the CD point, micro-crack density grows rapidly as the acoustic emission rate increases.

2.2 Size-effect research

Bieniawski [8] was the first researcher to study size effects in rock samples, specifically to estimate coal pillar strength. Pratt et al. [51] subsequently performed several tests with two different rock types, reporting that sample strength decreases as sample size increases and suggesting that laboratory sample strength is probably not representative of the strength of large volumes of in situ unjointed rock.

Hoek and Brown [26] suggested that the UCS of a rock sample with diameter d (in mm), σ_c , is related to the UCS of a 50-mm-diameter sample, σ_{c50} , according to:

$$\sigma_{cd} = \sigma_{c50} \left(\frac{50}{d} \right)^{0.18} \quad (3)$$

Hoek and Brown [26] further suggested that the strength reduction is due to the greater likelihood of failure through and around grains as more and more grains are included in the test sample. When a sufficiently large number of grains are included, then the strength value becomes constant.

Hawkins [25] noted that the Hoek and Brown [26] equation was based primarily on data for crystalline material and that only one of the ten samples was of a sedimentary rock; hence, the relationship shown in Eq. 3 may not be representative of all rock types. Hawkins [25] subsequently carried out comparative tests on seven sandstones and limestones, finding that maximum strength values for the sedimentary samples were obtained on cores of approximately 40–60 mm diameter, but that, unlike the results reported by Hoek and Brown [26], the UCS values were lower for cylinders that had both larger and smaller diameters than that of the 40–60 mm diameter range. In general, there was a 20–40% strength reduction from the maximum value—obtained for 54- or 38-mm-diameter cores—to the value obtained for the largest diameter core of 150 mm; for the 12.5-mm-diameter cores, the loss in strength was 45–65%. Hawkins [25] concluded that the Hoek and Brown [26] equation (Eq. 3) did not hold for sedimentary rocks.

Thuro et al. [54] tested a coarse-grained two-mica granite, a fine-grained amphibolite and a fine-grained clastic limestone, finding that size only had a marginal effect on UCS within the tested diameter range (45–80 mm for amphibolite and limestone and 45–110 mm for granite).

Yoshinaka et al. [61], who found significant differences in the relationship between the UCS and sample diameter depending on rock type, proposed rewriting the Hoek and

Brown [26] equation in the following general form, using the coefficient k as a variable exponent:

$$\sigma_c = \sigma_{c50} \left(\frac{d}{d_{50}} \right)^{-k} \quad (4)$$

where σ_{c50} is the UCS of standard-sized samples and σ_c is the UCS of samples with the same shape but an arbitrary diameter d (in mm). The value of the exponent k ranges between 0.1 and 0.3 for homogenous hard rock and between 0.3 and 0.9 for weathered rock [61]. Figure 2 illustrates this concept of variable strength reductions depending on rock type and level of weathering.

In their research into size effects, Masoumi et al. [44] detected a dual size effect: a general effect, when strength decreases with increasing sample diameter, and a reverse effect, when strength increases with increasing sample diameter. Note that the dual size effect was not first identified by Masoumi [43] or by Hawkins [25], but by Nishimatsu et al. [47], from UCS tests on a number of different igneous rocks.

Given this dual size effect, Masoumi et al. [44] proposed a unified size-effect law (USEL) that was capable of capturing both an increase in strength with diameter for smaller cores and a decrease in strength with diameter for larger cores. Verified against UCS results for various sedimentary rocks, the USEL showed good agreement for model outputs with experimental data.

To fit the size effect when strength decreases with increasing sample diameter (the general size effect), Bazant [5] proposed the following equation for the size-effect law based on the fracture energy model:

$$\sigma_N = \frac{Bf_t}{\sqrt{1 + (d/\lambda d_0)}} \quad (5)$$

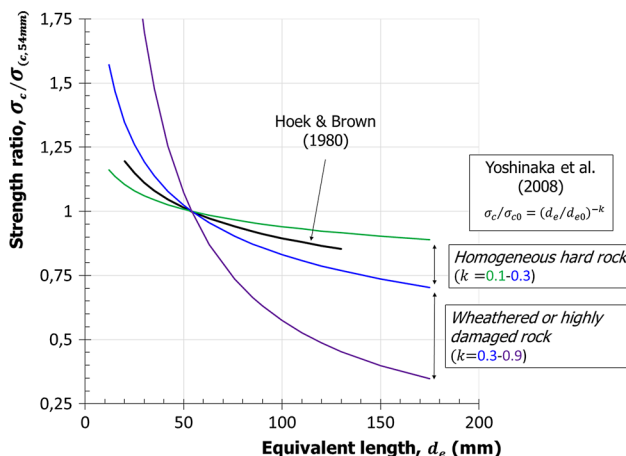


Fig. 2 Size-effect relationships for intact rock UCS, as proposed by Yoshinaka et al. [61], with the Hoek and Brown [26] relationship depicted for comparison purposes. Modified from Pierce et al. [49]

where σ_N is nominal strength, B and λ are dimensionless material constants, f_t is strength for a sample of negligible size that may be expressed in terms of an intrinsic strength, d is sample size, and d_0 is maximum grain size. In this equation Bf_t sets the strength level, whereas $d/\lambda d_0$ influences the rate of strength variation with size.

Bazant [6] later incorporated the concept of fractals into fracture energy, developing a fractal fracture size-effect law (FFSEL) to fit the reverse size effect:

$$\sigma_N = \frac{\sigma_0 \cdot d^{(d_f-1)/2}}{\sqrt{1 + (d/\lambda d_0)}} \quad (6)$$

where σ_0 is strength for a sample of negligible size that may be expressed in terms of an intrinsic strength and d_f is the fractal dimension; the remaining parameters, namely d , d_0 and λ , are the same as in Eq. 5. Carpinteri et al. [11] also used this FFSEL, given that, within a certain range of sizes, fracture surfaces in materials like concrete or rock exhibit fractal (self-similar) characteristics. For very high fractal dimension values (well over 1), the reverse size effect is reflected by Eq. 6. Although the foundations for this approach may seem counterintuitive [6], the shape of the derived curves has been empirically verified [44].

Masoumi et al. [44] subsequently combined Eqs. 5 and 6 in the USEL to reproduce size-effect behaviour for various sample sizes. The intersection between these equations occurs when:

$$d_i = \left(\frac{Bf_t}{\sigma_0} \right)^{2/(d_f-1)} \quad (7)$$

Masoumi et al. [44] compared the USEL to data obtained for Gosford sandstone samples with diameters of 19–146 mm and also to data reported by Hawkins [25]. Like Hawkins [25], Masoumi et al. [44] found that the UCS increases as sample size increases up to a characteristic diameter, but from this point the UCS decreases as sample size increases.

As an explanation for the reverse size effect for small diameters, Masoumi et al. [44] hypothesized that surface flaws or imperfections developed during sample preparation may influence sample strength and fractal behaviour. Another possible explanation is that developing cracks are less likely to stabilize in small samples, since it is easier for such cracks to intersect the (free) sample surface. If this is indeed the case, then the ratio of sample size to grain size may play a role. This hypothesis remains to be tested in the future, once more data on rocks of different grain sizes become available.

While suggesting that the USEL approach was suitable for sedimentary rocks, and particularly for Gosford sandstone, Masoumi [43] also tested two granites (labelled

A and B in Fig. 3), for which values of the parameters needed to capture the general size effect but not the reverse size effect were fitted. Since overall results for the granites were not as conclusive as the results for the sedimentary rocks, Masoumi [43] did not explicitly propose using the USEL for igneous rocks. In Fig. 3, the general size effect was fit as proposed by Masoumi [43], whereas the reverse size effect was fitted by the authors of this paper.

Seminal studies by Mogi [45], Obert and Duvall [48] and John [29] on shape effects on rock strength indicate that the strength of constant diameter rock cylindrical samples tends to decrease with increasing slenderness (length-to-diameter ratio) and that, for slenderness ratios over 2 or 2.5 (depending on rock type), a reasonably constant strength value is achieved. This observation has led to the establishment of current standards [4, 27]. More recent studies by Hawkins [25] and Tuncay and Hasancebi [57] have basically confirmed previous observations, and some formulae have been proposed for rock sets for which

tests have been performed. A different trend is observed for deformability, with the elastic Young's modulus values increasing with slenderness [54], even if this trend is not always that clear [31]. The scope of the research described here is limited to size effects.

3 Granite, samples and sample preparation

3.1 Blanco Mera granite

Samples of Blanco Mera, a bright, white, coarse-grained (1–6 mm) granite, were obtained from a quarry located in Lugo (NW Spain). Blanco Mera has been widely tested in the laboratory [1, 3], although not for size effects.

The samples were examined under an optical microscope to evaluate the geological nature of the rock (see Fig. 4 and Table 1). The average density of this material was found to be 2.60 g/cm^3 .

3.2 Sample diameters and number

The diameters of the tested cylindrical samples ranged from 14 to 100 mm. Although for uniaxial testing, the ISRM [27] recommends a sample height that is 2.5–3 times the diameter, a ratio of 2 was chosen for this research, as do other standards such as ASTM [4], some size-effect studies (Masoumi et al. [44]) and another study of the same granite by the authors of this paper [3].

The number of tests performed for each diameter (Table 2) is based on the fact that strength variability in smaller samples tends to be higher than in larger samples [43]. Figure 5 depicts the full set of tested samples.

The ISRM [27] also suggests that sample size should be at least ten times the size of the largest grain in the rock.

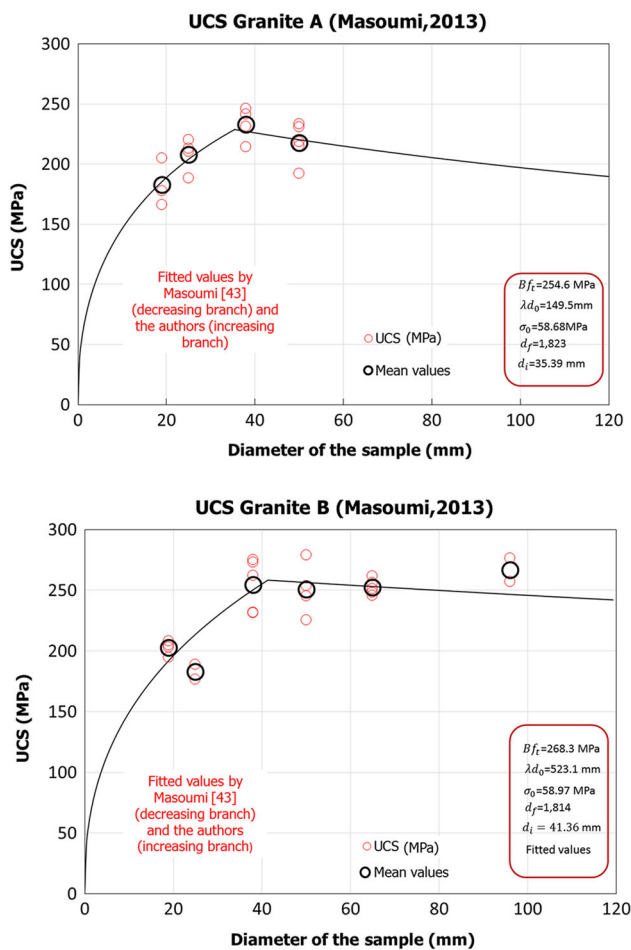


Fig. 3 Peak strength results for UCS tests for two granites, A and B, as obtained by Masoumi [43]. Values fitted by Masoumi [43] for the decreasing (*general size effect*) branch and by the authors for the increasing (*reverse size effect*) branch

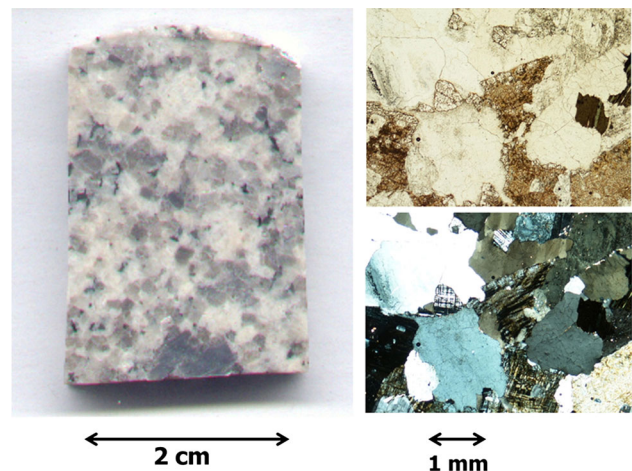


Fig. 4 Petrographic analysis of rock samples showing hand samples and thin section in white and polarized light. Source: Arzúa and Alejano [3]

Table 1 Quantitative modal analysis Source: Alejano et al. [1]

Mineral phases	Modal (%)
Quartz	20
Alkaline feldspar	27
Plagioclase	35
Biotite	5
Muscovite	7
Sericite	1
Chlorites	4
Opaques	–
Accessories	<1

Table 2 Tests for different Blanco Mera sample diameters

Tests (n = 28)	Sample diameter (mm)
10	14
10	30.1
6	54.7
2	100

This recommendation was disregarded, since it implied a minimum Blanco Mera sample diameter larger than 60 mm, which would not have allowed us to observe the reverse size effect.

3.3 Sample preparation

The samples were prepared in accordance with ISRM guidelines [27], except where otherwise noted. As stated above, sample diameter was variable and a height-to-

diameter ratio of 2 was used. Samples were not saturated before testing. The ends of the samples were flat within 0.02 mm. Loading on the samples was increased continuously at a stress rate of 0.5–1 MPa/s, it being aimed to finish each test in 5–10 min.

4 Laboratory tests

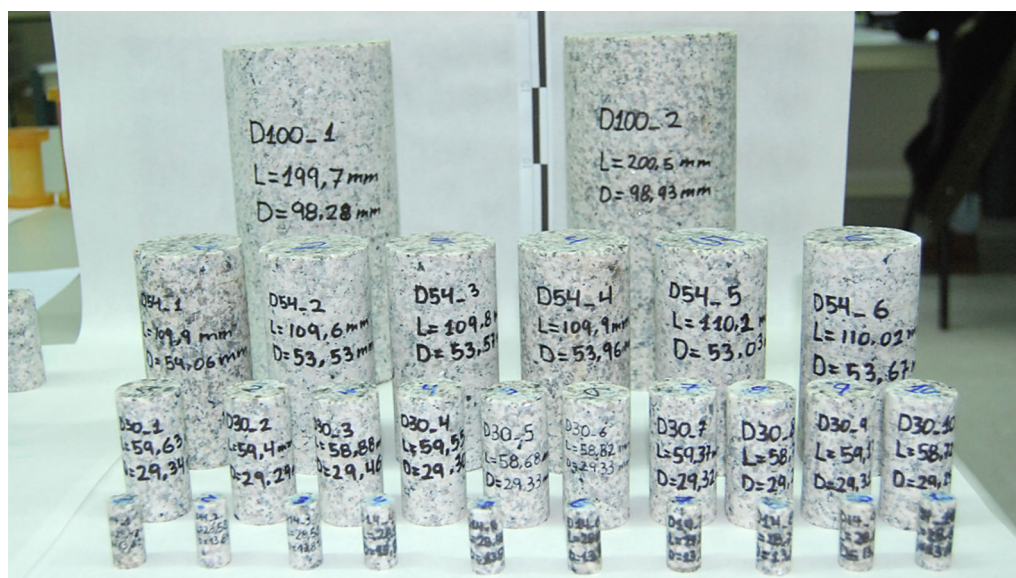
4.1 Equipment

A servo-controlled compression machine with a 200-tonne loading capacity was used for testing. Sample deformation was measured using linear variable differential transformers (LVDTs).

Axial strain was measured by attaching two LVDTs to the lower plate of the frame (Fig. 6a), in such a way that lower plate displacement was recorded by the LVDTs (the upper plate remained fixed). Lateral strain was measured using two devices, one for the larger samples (54 and 100 mm) and the other for the smaller samples (14 and 30 mm), which are depicted in Fig. 6b and c, respectively. The mechanical device for the larger samples measured sample diametrical strain using two LVDTs and that for the smaller samples was a ring holding up to four LVDTs as two diametrically opposed pairs, used because the first measurement device was not self-supporting for these small sample sizes.

4.2 Data processing

Data were processed in line with the recommendations of the ISRM [27], except where otherwise noted.

**Fig. 5** Set of Blanco Mera samples with diameters between 14 and 100 mm before testing

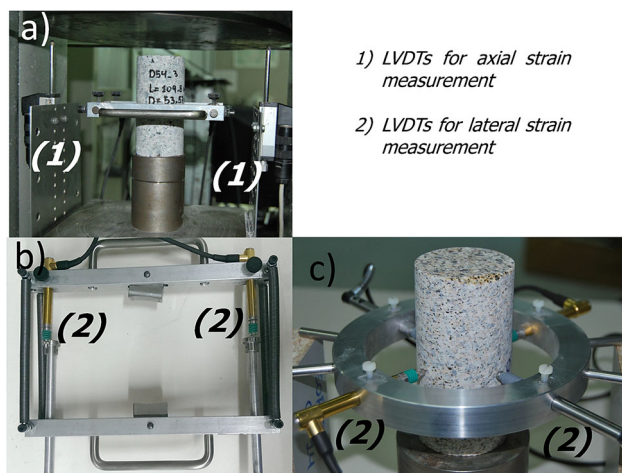


Fig. 6 a LVDTs used for strain measurements. b LVDTs used for lateral strain measurement. c Ring support for LVDTs for smaller samples

Of the various approaches to computing Young's moduli (average, secant or tangent), we calculated the average Young's modulus, E_{av} , from the linear portion of the axial stress–axial strain curve between 30 and 65% peak strength. The average Young's modulus was thus computed as:

$$E_{av} = \frac{\Delta\sigma}{\Delta\varepsilon_1} = \frac{\sigma_{65\%} - \sigma_{30\%}}{\varepsilon_{65\%} - \varepsilon_{30\%}} \quad (8)$$

where the $\sigma_{\%}$ values were calculated from a percentage of the UCS and the $\varepsilon_{\%}$ values reflected the axial strains at the corresponding stress levels.

The Poisson ratio, ν , was calculated as:

$$\nu = \frac{-E \cdot \Delta\varepsilon_3}{\Delta\sigma_1} \quad (9)$$

where E is Young's modulus, $\Delta\varepsilon_3$ is the change in radial strain from 20 to 40% peak strength, and $\Delta\sigma_1$ is the absolute difference between the corresponding stress levels. Volumetric strain, ε_v , was calculated as shown in Eq. 2.

5 Results

Below we present the UCS test results for 14-, 30-, 54- and 100-mm-diameter samples, with particular focus on the size effects associated with the following geomechanical parameters: peak strength, Young's modulus, Poisson's ratio, CI and CD. Results are summarized in Table 3; omitted are unreliable Poisson's ratio, CI and CD values arising from LVDT sliding problems during strain measurements.

5.1 Size effect on UCS

Table 4 shows means and standard deviations for the UCS results by diameter size. A significant level of data variability (in both absolute and relative terms) was observed, particularly for the smaller diameters. We therefore investigated the normality of the data, but only for the two smallest diameters, as a limited number of data points were available for the larger diameters.

The Kolmogorov–Smirnov statistical nonparametric test compares a sample with a reference probability distribution, for instance, a normal distribution. We used the Lilliefors [39] variant of this test because the mean and standard deviation of the hypothesized normal distribution were not 0,1. If the test statistic was larger than the critical value (0.262), the null hypothesis that the data were normally distributed could be rejected at a significance level of 0.05. In our case, for the ten values corresponding to the 14- and 30-mm-diameter samples, the null hypothesis could not be rejected since the test statistics (0.2012 and 0.2044, respectively) were smaller than the critical value (Fig. 7). This means that it cannot be stated that the data are not normally distributed. They probably are.

Peak strength size effects for the UCS results are plotted in Fig. 8. A strong reverse size effect—as observed by Masoumi et al. [44]—is evident: up to a diameter of 54 mm, peak strength increases as sample size increases, but above 54 mm, in line with more classical models [26], peak strength decreases as sample size increases.

The USEL approach proposed by Masoumi [43] was used to fit parameters to the values obtained for the studied samples (Fig. 8). The results point to a rather good fit, particularly for the average values for each diameter. Overall trends in the behaviour of the granite are consistent with those first identified by Nishimatsu et al. [47] and later confirmed by Hawkins [25] and Masoumi et al. [43, 44].

It can also be observed that Blanco Mera's parameter values (Table 5) are of the same order of magnitude as those obtained for the granites studied by Masoumi [43] (see Fig. 3). The USEL model fitted the data very well for granite A and Blanco Mera, as evidenced by high R^2 values, but less well for granite B.

5.2 Size effect on Young's modulus

Young's modulus results for each of the tested samples are shown in Table 3 above and plotted in Fig. 9; means and standard deviations are listed in Table 6.

It can be observed that variability (in both absolute and relative terms) was greater for the smaller samples, although relative variations in Young's modulus were less than in the UCS for all the diameters. Young's modulus

Table 3 Key geomechanical parameter results for all 28 tested samples: peak strength (UCS), Young's modulus (E), Poisson's ratio (ν), CI and CD

Sample	Diameter (mm)	UCS (MPa)	E (GPa)	ν –	CI (MPa)	CD (MPa)
D14_1	13.82	37.33	13.07	0.15	10.04	24.68
D14_2	13.84	59.43	15.55	0.11	14.84	36.41
D14_3	13.81	106.35	18.94	0.19	11.45	68.63
D14_4	13.82	34.73	12.70	–	–	–
D14_5	13.82	61.53	17.51	0.08	17.55	43.53
D14_6	13.87	49.51	16.89	0.09	–	40.91
D14_7	13.86	68.00	16.25	0.24	12.39	–
D14_8	13.87	55.53	18.45	0.08	14.93	34.42
D14_9	13.88	62.32	14.56	0.26	–	–
D14_10	13.90	89.10	24.73	0.24	13.14	58.92
D30_1	29.34	125.99	34.14	0.23	45.92	90.71
D30_2	29.29	69.29	17.98	0.05	28.24	47.53
D30_3	29.46	78.99	21.93	0.06	31.11	58.05
D30_4	29.30	66.00	19.47	0.33	–	52.05
D30_5	29.33	101.36	24.94	0.17	28.46	48.82
D30_6	29.33	90.11	25.11	0.08	24.89	71.02
D30_7	29.32	91.04	25.64	0.09	40.77	63.84
D30_8	29.27	73.91	21.19	0.05	31.34	48.82
D30_9	29.31	78.88	20.98	0.23	35.77	52.55
D30_10	29.25	64.45	19.93	0.12	26.86	53.84
D54_1	54.06	122.08	39.56	0.21	40.14	75.10
D54_2	53.53	107.53	37.31	0.22	30.65	89.75
D54_3	53.58	108.68	33.56	0.27	42.09	69.24
D54_4	53.96	131.76	37.14	0.23	57.94	72.68
D54_5	53.03	122.90	37.14	0.21	43.88	81.65
D54_6	53.67	139.39	39.76	0.2	69.93	97.04
D100_1	98.28	107.88	52.52	0.24	38.63	63.67
D100_2	98.93	116.93	55.85	0.32	38.29	76.65

Table 4 Peak strength means and standard deviations for the UCS tests

Diameter (mm)	Number of tested samples	Mean (MPa)	Standard deviation (MPa)	% variation
14	10	62.38	20.72	33.21
30	10	84.00	17.96	21.39
54	6	122.06	11.44	9.37
100	2	112.41	4.53	4.03

clearly increased as sample size increased, with no evident reverse size effect.

5.3 Size effect on Poisson's ratio

Poisson's ratio results for each of the tested samples are shown in Table 3 above and plotted in Fig. 10; means and standard deviations are listed in Table 7.

Data variability was high, most especially for the smaller samples, and scattering increased as the sample size decreased. Although a slight positive trend with size was evident that corroborates Masoumi [43] results for sandstone, given the great variability of the data, it is not possible to conclude that Poisson's ratio was significantly different from one sample size to another.

5.4 Size effect on CI and CD

CI and CD results for all the tested samples, listed in Table 3 above, can be interpreted either as absolute values, independent of the UCS, or as a proportion of the UCS. UCS, CI and CD data in absolute terms are plotted in Fig. 11, which shows that the initial reverse size effect, followed by strength decreasing with size, not only occurs for peak strength but also for these brittle

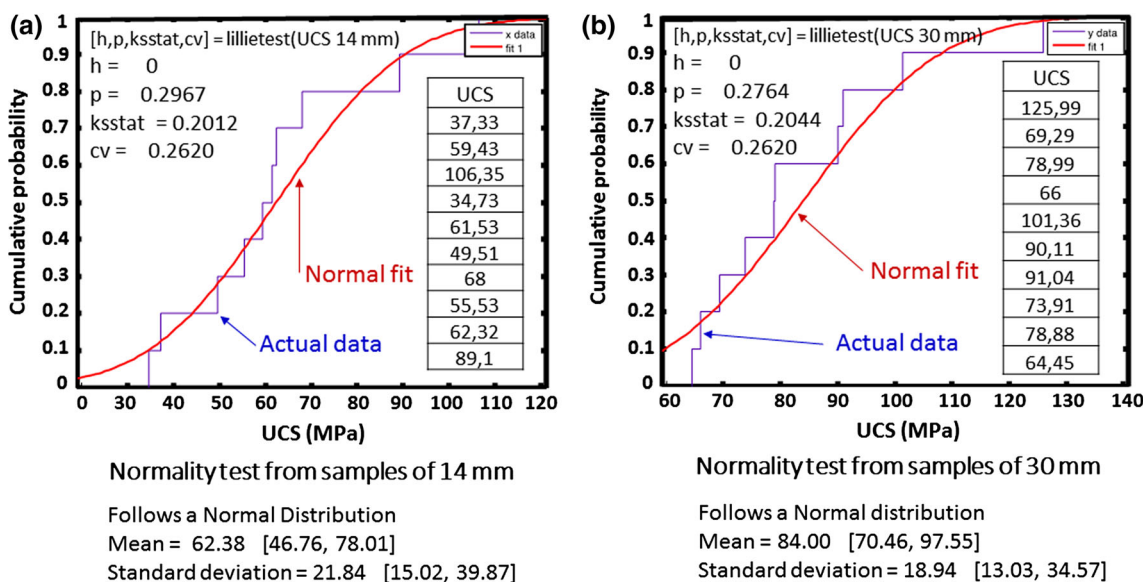


Fig. 7 Lilliefors normality tests for UCS results for the 14-mm and 30-mm-diameter samples, showing theoretical and real cumulative probability density functions and demonstrating that both sets of samples are normally distributed

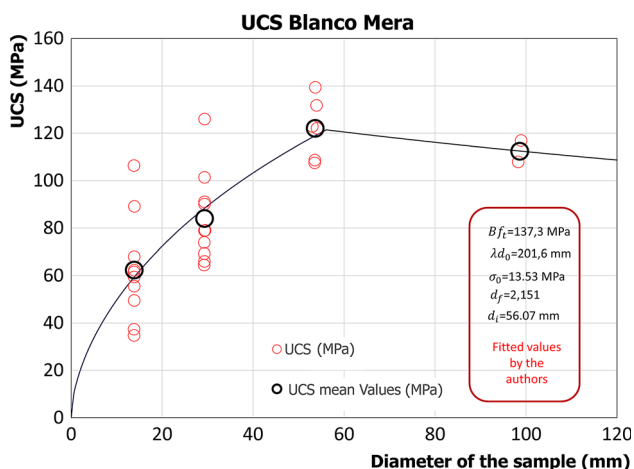


Fig. 8 Peak strength results for the UCS tests for Blanco Mera granite. USEL approach parameters fitted by the authors using the MATLAB fitting tool

cracking parameters, whose trends seem to follow a similar pattern.

As the references of this study clearly show, many studies have been published regarding the size effects of strength on intact rock; however, lacking are insights into size effects on CI and CD. Figure 11 suggests that trends observed for strength could probably be extended to crack parameters.

Martin [40] published a detailed study on Lac du Bonnet granite, whose results in terms of size effects on UCS, CD and CI, presented in Fig. 12, show a similar increasing–decreasing trend, particularly for CD, although the range of values recorded was not as wide as in our case. Martin [40] interpreted the results by suggesting that CD

and CI should be approximately constant as a function of the sample diameter. However, since Martin [40] focused on samples of sizes larger than the standard 50 mm diameter, this interpretation may under-represent the reverse size effect.

Based on trend similarity for UCS, CI and CD, the USEL model was fitted to CI and CD. Figure 13 shows all the original data points and average values as well as USEL fit to the CI and CD values and the UCS USEL model scaled by the average CI/UCS = 0.33 and CD/UCS = 0.68 ratios. Table 8 summarizes the parameters for all these fits and their associated R² values.

Figure 13 shows that the USEL model fitted the CI and CD results with quite good regression coefficients for average values of these parameters for all sample sizes. Additionally, scaling the UCS USEL model by the average CI/UCS = 0.33 and CD/UCS = 0.68 ratios provided a good approximation to the best fitting USEL models for these parameters.

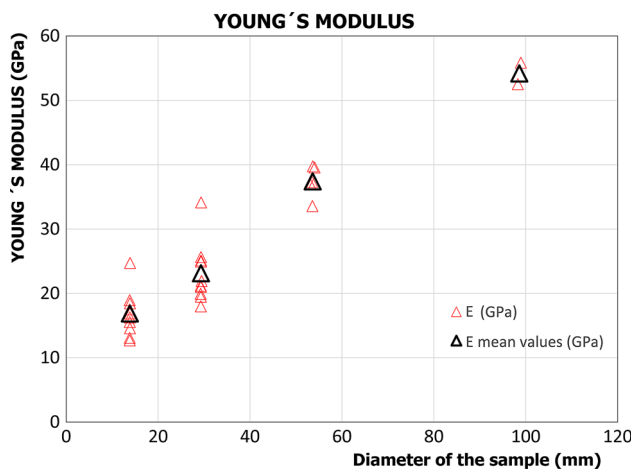
The CI/UCS and CD/UCS ratios, as determined independently for each sample, are plotted in Fig. 14. It can be observed that there were no significant differences between the average values for different sizes, most particularly for CD, and also that only for the smallest sample size was there a slight drop in the CI/UCS ratio.

6 Discussion

The Blanco Mera granite follows the USEL model proposed by Masoumi et al. [44] for UCS, CI and CD, showing a trend of strength increasing with sample

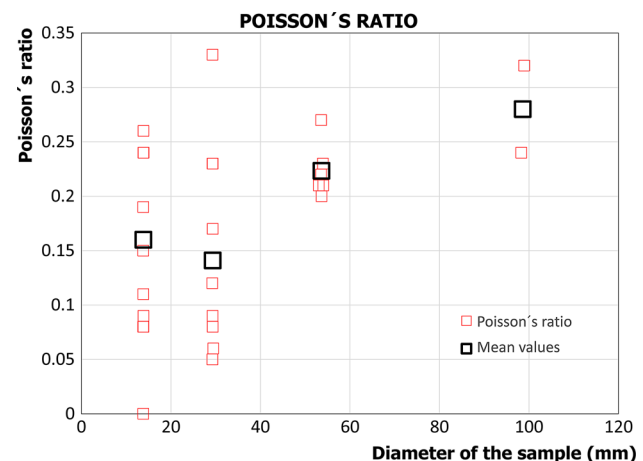
Table 5 USEL approach parameters fitted by Masoumi [43] and the authors for granites A and B and by the authors for the Blanco Mera granite using the MATLAB fitting tool

Parameters	Granite A Masoumi [43] and this research	Granite B Masoumi [43] and this research	Blanco Mera granite (this research)
$B \cdot f_i$ (MPa)	254.6	268.3	137.3
$\lambda \cdot d_0$ (mm)	149.5	523.1	201.6
σ_0 (MPa)	58.68	58.97	13.53
d_f	1.823	1.814	2.151
d_i (mm)	35.39	41.36	56.07
R^2 (all values)	0.57	0.63	0.62
R^2 (mean values)	0.95	0.74	0.98

**Fig. 9** Young's modulus results for the different sample diameters tested**Table 6** Young's modulus means and standard deviations for the UCS tests

Diameter (mm)	Number of tested samples	Mean (GPa)	Standard deviation (GPa)	% variation
14	10	16.87	3.29	19.51
30	10	23.13	4.23	18.30
54	6	37.41	2.05	5.47
100	2	54.19	1.67	3.07

diameter followed by strength decreasing with sample diameter. Masoumi et al. [44] suggested that this behaviour could be explained by two mechanisms. The first—somewhat counterintuitive—mechanism, described by Bazant [6], is associated with rock multifractality. The second mechanism is sample weakening due to near-surface damage during sample preparation, which has a disproportionate effect on smaller samples with a higher surface area-to-volume ratio [58].

**Fig. 10** Poisson's ratio results for the different sample diameters tested

In smaller samples containing very few mineral grains, initial cracks growing at the scale of individual grains can easily connect to the sample surface. Failure mechanisms [36] are highly dependent on the arrangement of a few grains, with an outcome of extreme variability in the observed results. Consider, for instance, smaller sizes of Blanco Mera granite as depicted in Fig. 15, whose significant heterogeneity may explain the greater results variability observed for smaller samples. A 14-mm-diameter sample may consist of a single large feldspar grain or of many tens of mineral grains with different compositions, whereas a 100-mm-diameter sample will have similar grain size and composition distributions. This mechanism would explain the lower peak strength of smaller hard rock samples, like granite, with coarse grain crystals; note, however, that this mechanism may not operate for other rocks.

For samples with larger diameters, the general size effect has been widely explained by traditional approaches

Table 7 Poisson’s ratio means and standard deviations for the UCS tests

Diameter (mm)	Number of tested samples	Mean (GPa)	Standard deviation (GPa)	% variation
14	10	0.16	0.07	43.70
30	10	0.14	0.09	64.58
54	6	0.22	0.02	10.23
100	2	0.28	0.04	14.29

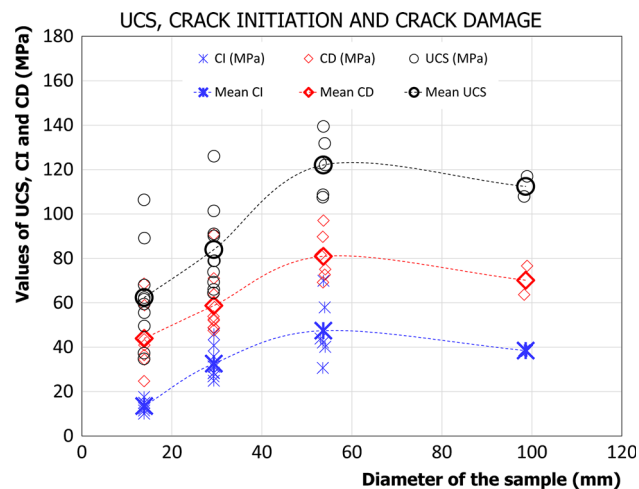


Fig. 11 Absolute values for CI, CD and UCS results for the different sample diameters tested

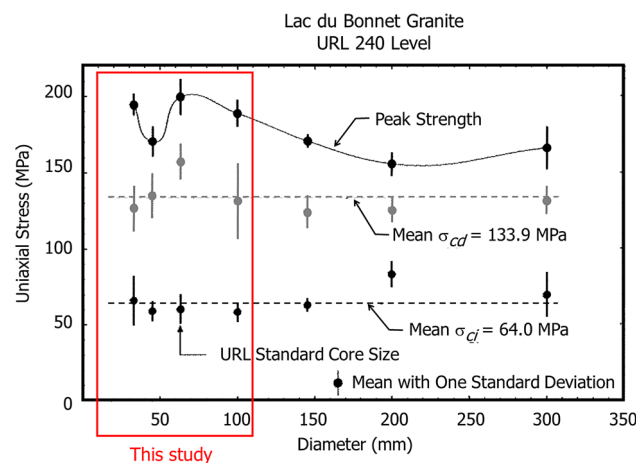


Fig. 12 Size effects on UCS, CD and CI for Lac du Bonnet granite as studied by Martin [40], with the scope of this research (diameters up to 100 mm) indicated by a red rectangle

[8, 26, 51, 61]. The weakest link paradigm can also explain this mechanism.

Young’s modulus was found to consistently increase with sample diameters from 14 to 100 mm (see Fig. 9). Damage during sample preparation can at least partially explain this trend: smaller samples have relatively greater surface areas and, therefore, undergo more damage per unit

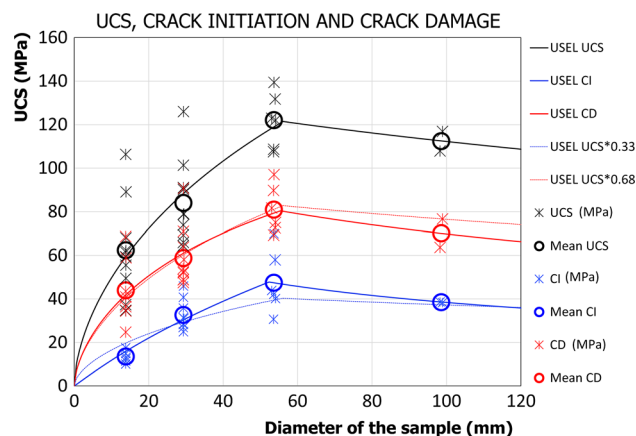


Fig. 13 UCS, CI and CD results and average values for each sample diameter. The USEL was first fitted to UCS, CD and CI (continuous lines). Then, CI and CD were also fitted as the UCS USEL fit multiplied by the average CI/UCS and CD/UCS values, respectively (dotted lines)

Table 8 USEL approach parameters as fitted by the authors for the CI, CD and UCS results for Blanco Mera granite and USEL CI and CD parameters computed as a fraction of the UCS

Parameters	CI USEL fit	CD USEL fit	UCS USEL fit	CI USEL UCS*0,33	CD USEL UCS*0,68
$B \cdot f_t$ (MPa)	75.76	104.2	137.3	45.54	93.59
$\lambda \cdot d_0$ (mm)	34.5	81.52	201.6	201.6	201.6
σ_0 (MPa)	1.2	9349	13.53	4.49	9.22
d_f	3095	2201	2151	2151	2151
d_i (mm)	52.31	55.43	56.07	56.07	56.07
R^2 (all values)	0.72	0.54	0.63	0.59	0.31
R^2 (mean values)	0.98	0.98	0.98	0.81	0.92

volume. Moreover, smaller samples with higher damage densities could be expected to be less rigid. This result contradicts that of Pratt et al. [51], who reported the absence of a size effect on the Young’s modulus for a granodiorite and a quartz diorite. It also contradicts Simon and Deng [52], who reported that Young’s moduli tend to decrease as size increases, and Masoumi [43], who, regarding granites, stated the Young’s modulus initially decreased and then increased as a function of size. Our results are, however, consistent with those of Walton [59], who studied size effects in Stanstead granite. The different size effects observed for Young’s modulus in various studies highlight the need for more research into this issue.

Regarding the mechanistic processes that gave rise to the observed results, a seminal proposal by Fairhurst [19] indicated that, starting from elastic energy principles,

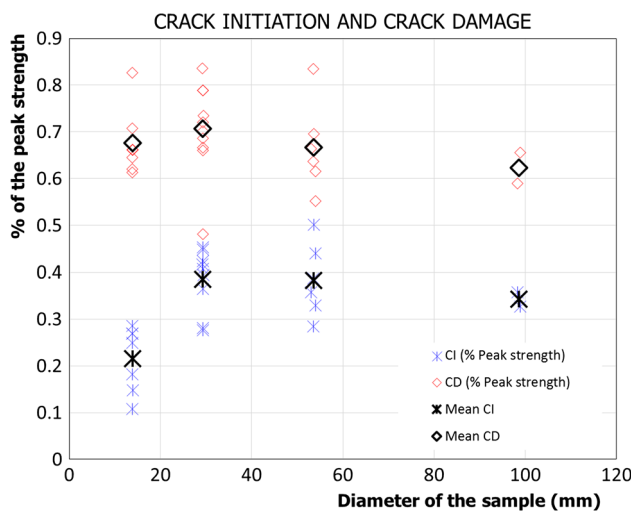


Fig. 14 CI and CD values relative to peak strength

strength and sample size can be expressed in the general form $LS^2 = \text{constant}$, where L is the length of the critical flaw (e.g. a pre-existing crack) and S is the strength of the tested sample. Thus, if the size of the critical flaw increases with sample size, then strength should decrease proportionally to $L^{-0.5}$. Studies on micro-crack morphogenesis, kinematics, dynamics, population statistics and observational techniques [36] indicate that increasing flaw size

(with increasing sample size) should decrease sample strength, i.e. it should induce the typical size effects.

However, mechanical phenomena governing the brittle behaviour of crystalline rocks are complex (they include crack growth, crack–crack and crack–pore interactions, crack coalescence, crystal plasticity, micro-fracturing, cataclastic flow, dislocation creep, dynamic recrystallization, diffusive mass transfer, particle size and distribution, grain boundary sliding, grain contact wear, grain corner crushing, the impact of softer minerals (like micas and clays), etc.) [7, 34, 35, 53, 55]. In view of this complexity, it is hardly surprising that no theoretical mechanistic approach has, to date, been able to accurately reproduce this behaviour and reflect size effects as demonstrated in our experiments or similar ones [25, 43].

A number of interesting studies have addressed some of the mentioned mechanisms using micromechanical analyses [15], mesoscale numerical analyses of lattice models based on fracture processing zones surrounding macro-cracks [21], crystal plasticity and micro-fracturing [55, 56], fractal theory [62], contact mechanics [30] and granular matter approaches [2, 12]. Although each of these approaches is capable of reproducing some interesting features, none has proved capable of representatively reproducing the USEL response.

One of the most promising approaches, from the field of particle mechanics, is the discrete element method [16], for

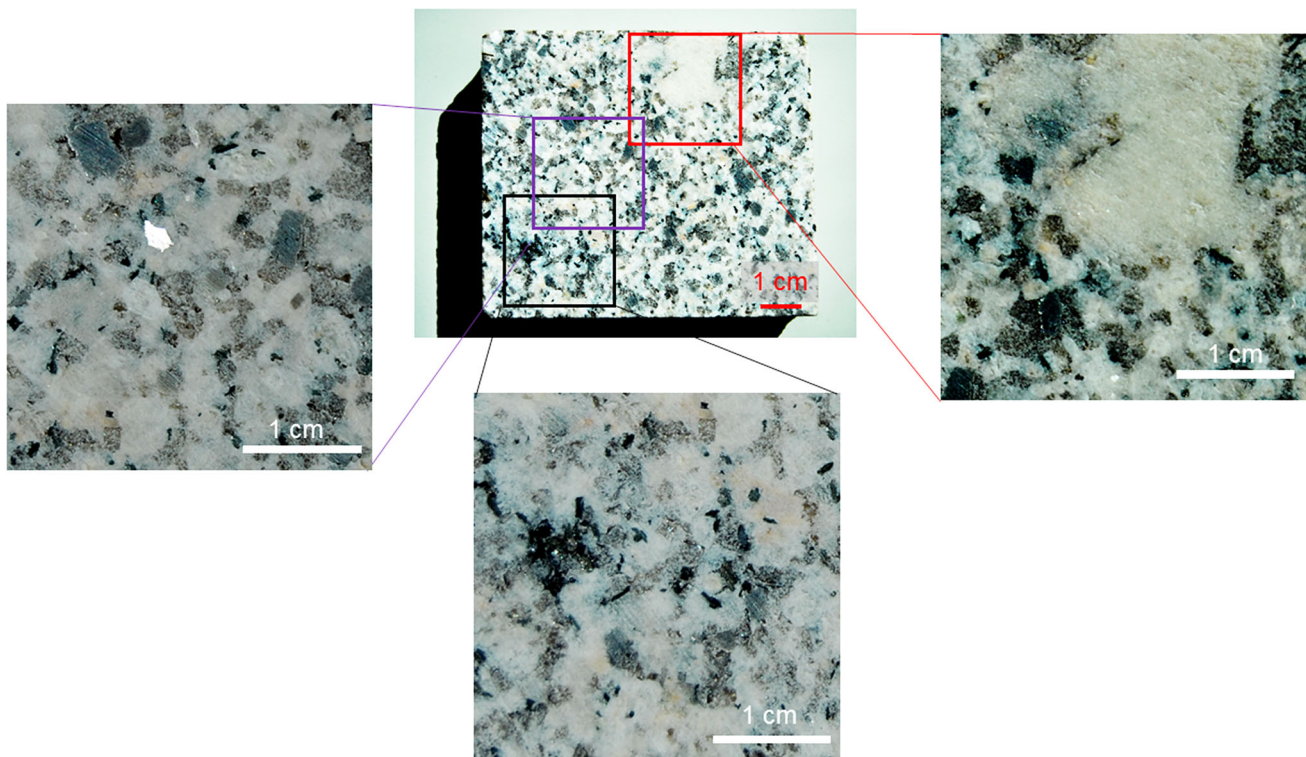


Fig. 15 A slab of Blanco Mera granite, 8 cm wide and 7 cm high, with detailed views of various zones showing heterogeneity

which the PFC code [28, 50] is often used. Studies at the fractured rock mass scale have been able to reasonably reproduce size-dependent strength results [16, 18, 42], but studies of small samples of intact rock have not yet produced size-dependent results [33]. New developments based on correlated random fields [38] may lead to improved reliability in the simulation of size effects using this kind of approach.

7 Conclusions

In this study of size effects on the geomechanical parameters of a Blanco Mera granite based on UCS testing results, we found a significant reverse size effect for smaller diameter samples: strength values increased as the sample size increased up to around a diameter of 54 mm and—as predicted by classical models [26]—decreased from this point.

This result is consistent with previous observations by various authors [25, 43, 44, 47] but disagrees with classical size-effect models for smaller sample sizes [8, 26, 61]. The best model found for capturing the observed trend in the UCS data was the USEL model proposed by Masoumi et al. [44]. Similar trends were noted for the brittle cracking strength thresholds, CI and CD.

The Young's modulus positively and consistently correlated with sample size, a finding that, again, is consistent with results for some studies [54, 59] but in disagreement with findings for other rocks [43, 51, 52]. It was not possible to draw any clear conclusions regarding the variability in Poisson's ratio results.

The significant variability in the results (particularly for small sample sizes) would suggest that future studies should be based on larger numbers of samples and also on larger numbers of different sample diameters.

Acknowledgements The authors thank the Spanish Ministry of the Economy and Competitiveness for funding this research, awarded under Contract Reference No. BIA2014-53368P, partially financed by means of ERDF funds from the EU. Ailish M. J. Maher is acknowledged for language editing of a version of this manuscript.

References

- Alejano LR, González J, Muralha J (2012) Comparison of different techniques of tilt testing and basic friction angle variability assessment. *Rock Mech Rock Eng* 45:1023–1035
- Andrade JE, Avila CF, Hall SA, Lenoir C, Viggiani G (2011) Multiscale modeling and characterization of granular matter: from grain kinematics to continuum mechanics. *J Mech Phys Solids* 59:237–250
- Arzúa J, Alejano LR (2013) Dilation in granite during servo-controlled triaxial strength tests. *Int J Rock Mech Min Sci* 61:43–56
- ASTM (2000) D7012 – 14. Standard Test Methods for Compressive Strength and Elastic Moduli of Intact Rock Core Specimens under Varying States of Stress and Temperatures
- Bažant ZP (1984) Size effect in blunt fracture: concrete, rock and metal. *J Eng Mech (ASCE)* 110:518–535
- Bažant ZP (1997) Scaling of quasi-brittle fracture: hypotheses of invasive and lacunar fractality, their critique and Weibull connection. *Int J Fract* 83:19–40
- Bennett KC, Berla LA, Nix WD, Borja RI (2015) Instrumented nano-indentation and 3D mechanistic modeling of a shale at multiple scales. *Acta Geotech* 10:1–14
- Bieniawski ZT (1967) The effect of specimen size on compressive strength of coal. *Int J Rock Mech Min Sci* 5:325–335
- Brace WF (1964) Brittle fracture on rocks. *Proc. Int. Conf., State of stress in the Earth's Crust.* (ed Judd), 111–180. Elsevier, New York
- Brace WF, Paulding B, Scholz C (1966) Dilatancy in the fracture of crystalline rocks. *J Geophys Res* 71:3939–3953
- Carpinteri A, Chiaia B, Ferro G (1995) Size effects on nominal tensile strength of concrete structures: multifractality of material ligaments and dimensional transition from order to disorder. *Mater Struct* 28:311–317
- Cil MB, Buscarera G (2016) DEM assessment of scaling laws capturing the grain size dependence of yielding in granular soils. *Granul Matter* 18:36. doi:10.1007/s10035-016-0638-9
- Diederichs MS (2007) The 2003 CGS Geocolloquium Address: damage and spalling prediction criteria for deep tunnelling. *Can Geotech J* 44:1082–1116
- Diederichs MS, Martin CD (2010) Measurement of spalling parameters from laboratory testing. In: *Rock mechanics and environmental engineering. Paper presented at Proceedings of Eurock 2010*; pp: 323–326. Lausanne, Switzerland
- Duan K, Kwok CY, Tham LG (2015) Micromechanical analysis of the failure process of brittle rock. *Int J for Numer and Anal Meth Geomech* 39:618–634
- Duan K, Kwok CY, Pierce M (2016) Discrete element method modeling of inherently anisotropic rocks under uniaxial compression loading. *Int J for Numer Anal Meth Geomech* 10:1150–1183
- Eberhardt E, Stead D, Stimpson B, Read R (1998) Identifying crack initiation and propagation thresholds in brittle rocks. *Can Geotech J* 35:222–233
- Esmaili K, Hadjigeorgiou F, Grenon M (2015) Capturing the complete stress-strain behaviour of jointed rock using a numerical approach. *Int J for Numer Anal Meth Geomech* 39:1027–1044
- Fairhurst C (1972) Fundamental considerations relating to the strength of rock. Technical Report Colloquium on Rock Fracture, Ruhr Universität, Bochum, Germany
- Ghazvinian E, Diederichs M, Martin D (2012) Identification of crack damage thresholds in crystalline rock. In: *Proceedings of EUROCK 2012. International Society for Rock Mechanics*
- Grégoire D, Verdon L, Lefort V, Grassl P, Saliba J, Regoin JP, Loukili A, Pijaudier-Cabot G (2015) Mesoscale analysis of failure in quasi-brittle materials: comparison between lattice model and acoustic emission data. *Int J for Numer and Anal Meth Geomech* 39:1639–1664
- Griffith AA (1921) The phenomena of rupture and flow in solids. *Phil Trans Roy Soc Lond A* 221:163–198
- Griffith AA (1924) Theory of rupture. *Proceeding 1st International Congress Applied Mechanics.* Deft. 55–63
- Hakala M, Heikkilä E (1997) Laboratory testing of Olkiluoto mica gneiss in borehole OL-KR10. Posiva Working Report 97-07e. Posiva Oy, Helsinki
- Hawkins AB (1998) Aspects of rock strength. *Bull Eng Geol Env* 57:17–30

26. Hoek E, Brown ET (1980) *Underground excavations in rock*. IMM, London
27. ISRM (2007) *The complete ISRM suggested methods for rock characterization, testing and monitoring: 1974–2006*. R. Ulusay & J. A. Hudson (eds), Ankara, Turkey
28. Itasca Consulting Group (2010) *PFC2D and PFC 3D user's manual, ver. 4.0 and 3.0*. Minneapolis: Minnesota
29. John M (1972) The influence of length to diameter ratio on rock properties in uniaxial compression: a contribution to standardization in rock mechanics testing. Rep S Afr CSIR No ME1083/5
30. Johnson KL (1985) *Contact mechanics*. Cambridge University Press, London
31. Kahraman S, Alber M (2006) Estimating unconfined compressive strength and elastic modulus of a fault breccia mixture of weak blocks and strong matrix. *Int J Rock Mech Mining Sci* 43:1277–1287
32. Korinets A, Alehossein H (2002) On the initial non-linearity of compressive stress-strain curves for intact rock. *Rock Mech Rock Eng* 35:319–328
33. Koyama T, Jing L (2007) Effects of model scale and particle size on micro-mechanical properties and failure processes of rocks—a particle mechanics approach. *Eng Anal Bound Elem* 31:458–472
34. Kranz RL (1979) Crack-crack and crack-pore interactions in stressed granite. *Int J Rock Mech Min Sci Geomech Abstr* 16:37–47
35. Kranz RL (1979) Crack growth and development during creep of Barre granite. *Int J Rock Mech Min Sci Geomech Abstr* 16:23–35
36. Kranz RL (1983) Microcracks in rocks: a review. *Tectonophysics* 100:449–480
37. Lajtai EZ (1974) Brittle fracture in compression. *Int J Fract Mech* 10:525–536
38. Le Goc R, Bouzeran L, Darcel C, Mas-Ivars D (2015) Using correlated random fields for modeling the spatial heterogeneity of rock. In: *Proceedings Eurock 2015, Salzburg, Austria*
39. Lilliefors H (1967) On the Kolmogorov-Smirnov test for normality with mean and variance unknown. *J Am Stat Assoc* 62:399–402
40. Martin CD (1993) *The Strength of massive Lac du Bonnet Granite around underground openings*. Ph.D. Dissertation. University of Manitoba
41. Martin CD, Chandler NA (1994) The progressive fracture of Lac du Bonnet granite. *Int J Rock Mech Min Sci Geomech Abstr* 31:643–659
42. Mas Ivars D, Pierce ME, Darcel C, Reyes-Montes J, Potyondy DO, Paul Young R, Cundall PA (2011) The synthetic rock mass approach for jointed rock mass modelling. *Int J Rock Mech Min Sci* 48:219–244
43. Masoumi H (2013) *Investigation into the mechanical behaviour of intact rock at different sizes*. Ph.D. Dissertation, University of New South Wales
44. Masoumi H, Saydam S, Hagan PC (2016) Unified size-effect law for intact rock. *Int J Geomech (ASCE)* 16(2):04015059
45. Mogi K (1962) The influence of the dimensions of specimens on the rock fracture strength of rocks. *Bull Earth Res Inst Tokyo Univ* 40:175–185
46. Nicksiar M, Martin CD (2012) Evaluation of methods for determining crack initiation in compression tests on low-porosity rocks. *Rock Mech Rock Eng* 45:607–617
47. Nishimatsu Y, Yamagushi U, Motosugi K, Morita M (1969) The size effect and experimental error of the strength of rocks (in Japanese). *J Min Mat Proc Inst Jpn* 18:1019–1025
48. Obert L, Duvall WI (1967) *Rock mechanics and the design of structures in rock*. Wiley, London, p 650
49. Pierce M, Gaida M, DeGagne O (2009) Estimation of rock block strength. In: *Proceedings 3rd CANUS Rock Mechanics Symposium, Toronto*
50. Potyondy DO, Cundall PA (2004) A bonded-particle model for rock. *Int J Rock Mech Min Sci* 41:1329–1364
51. Pratt HR, Black AD, Brown WS, Brace WF (1971) The effect of the specimen size on the mechanical properties of unjointed diorite. *Int J Rock Mech Min Sci* 9:513–529
52. Simon R, Deng D (2009) Estimation of scale effect of intact rock using dilatometer test results. In: *Proceedings of the Geohalifax*
53. Tapponnier P, Brace WF (1976) Development of stress-induced microcracks in Westerly granite. *Int J Rock Mech Min Sci Geomech Abstr* 13:103–112
54. Thuro K, Pilininger RJ, Záh S, Schütz S (2001) Scale effects in rock strength properties. In: *Proceedings of the ISRM Regional Symposium, EUROCK 2001, Rock Mechanics a Challenge for Society, Espoo, Finland*
55. Tjioe M, Borja RI (2015) On the pore-scale mechanisms leading to brittle and ductile deformation behavior of crystalline rocks. *Int J for Numer and Anal Meth in Geomech* 39:1165–1187
56. Tjioe M, Borja RI (2016) Pore-scale modeling of deformation and shear band bifurcation in porous crystalline rocks. *Int J Numer Meth Eng* 108:183–212
57. Tuncay E, Hasancebi N (2009) The effect of length to diameter ratio of test specimens on the uniaxial compressive strength of rock. *Bull Eng Geol Environ* 68:491–497
58. Vutukuri VS, Lama RD, Saluja SS (1974) *Handbook on mechanical properties of rocks*. Trans Tech Publications, Bay Village
59. Walton G (2016) Scale effects observed in compression testing of Stanstead granite including post-peak strength and dilatancy. Personal communication
60. Wawersik WR, Fairhurst C (1970) A study of brittle rock fracture in laboratory compression experiments. *Int J Rock Mech Min Sci Geomech Abstr* 7:561–575
61. Yoshinaka R, Osada M, Park H, Sasaki T, Sasaki K (2008) Practical determination of mechanical design parameters of intact rock considering scale effect. *Eng Geol* 96:173–186
62. Zhang K, Cao P, Ma G, Wang W, Fan W, Li K (2016) Strength, fragmentation and fractal properties of mixed flaws. *Acta Geotech* 11:901–912
63. Zhao XG, Cai M, Wang J, Li PF, Ma LK (2015) Objective determination of crack initiation stress of brittle rocks under compression using AE measurement. *Rock Mech Rock Eng* 48(6):2473–2484